Oxygen Reactivity of an NADH Oxidase C42S Mutant: Evidence for a C(4a)-Peroxyflavin Intermediate and a Rate-Limiting Conformational Change†

T. Conn Mallett and Al Claiborne*

Department of Biochemistry, Wake Forest University Medical Center, Winston-Salem, North Carolina 27157

Received February 16, 1998; Revised Manuscript Received April 10, 1998

ABSTRACT: The flavoprotein NADH oxidase ($O_2 \rightarrow 2H_2O$) from *Enterococcus faecalis* 10C1 contains a cysteinyl redox center, in addition to FAD. We have proposed a cysteine-sulfenic acid (Cys-SOH) structure for the oxidized form of Cys42; the presence of this redox center is consistent with the stoichiometries reported for earlier reductive titrations of wild-type oxidase, and we have proposed that Cys42-SH plays a key role in the overall four-electron reduction of $O_2 \rightarrow 2H_2O$. To test these proposals, we provide in this report an analysis of the oxidative half-reaction of an oxidase mutant in which Cys42 is replaced by Ser. NADH titrations lead to direct flavin reduction with 1.05 equiv of NADH/FAD and give rise to the formation of a very stable E-$FADH_2$·NAD^+ complex. Kinetic analyses indicate that this species is catalytically competent, and its reactivity with O_2 has been analyzed in detail by stopped-flow spectrophotometry using both single-wavelength and diode-array modes of data acquisition. The combined results of this analysis demonstrate that replacement of Cys42 with Ser provides for an altered O_2 reduction stoichiometry in which H_2O_2, not $2H_2O$, is the product. The two subunits of the reduced enzyme·NAD^+ complex react with O_2 in an asymmetric mechanism, consistent with an alternating sites cooperativity model such as that proposed [Miller, S. M., Massey, V., Williams, C. H., Jr., Ballou, D. P., and Walsh, C. T. (1991) *Biochemistry 30*, 2600−2612] for mercuric reductase. An FAD C(4a)-hydroperoxide is identified as the primary oxygenated intermediate in reoxidation of the complex, but the reaction of O_2 with the complementary subunit does not proceed until full reoxidation has occurred at the primary subunit. To our knowledge, this is the first report of a C(4a)-peroxyflavin intermediate outside the flavoprotein monooxygenase class.

In the heme- and cytochrome-deficient enterococci and streptococci, the flavoprotein NADH oxidase (Nox)[1] catalyzes the direct reduction of $O_2 \rightarrow 2H_2O$ (*1*, *2*). In so doing, this unusual FAD-dependent enzyme performs two important functions: it regenerates the NAD^+ required for glycolysis in these homofermentative organisms (*3*), and it contributes indirectly to the antioxidant defense mechanisms of these bacteria by favoring direct tetravalent ($\rightarrow 2H_2O$) rather than univalent ($\rightarrow$superoxide) or bivalent ($\rightarrow H_2O_2$) reduction of O_2 (*4*). The enzyme has been purified from *Enterococcus faecalis* (*1*) and *Streptococcus mutans* (*5*), and the recombinant Noxs from *Streptococcus pyogenes* and *Streptococcus pneumoniae* have recently been prepared.[2] The *E. faecalis* Nox is a dimer of two identical 50 kDa subunits, each of which contains one FAD and a cysteinyl redox center; we have proposed that the oxidized form of this non-flavin redox center is a cysteine-sulfenic acid (Cys-SOH; *1*). Indirect support for this proposal comes from the earlier demonstration that the *E. faecalis nox* sequence (*6*) predicts a primary structure 44% identical to that of the *E. faecalis* NADH peroxidase (Npx; $H_2O_2 \rightarrow 2H_2O$); the peroxidase has been characterized extensively (*7*−*9*) and is the first example of a native protein which utilizes a stable Cys-SOH redox center, in concert with FAD, in catalysis. Cys42, which provides the Cys-SOH redox center in Npx, is absolutely conserved in all Nox sequences (*6*, *10*, *11*, footnote 3), this leads to the expectation that Cys42-SOH is the non-flavin redox center in *E. faecalis* Nox.

In the peroxidase, Cys42-S^-, the reduced thiolate form of Cys42-SOH, reacts directly with the H_2O_2 substrate in a nucleophilic attack facilitated by hydrogen-bonding interactions in the transition state between the peroxide oxygen(s) and the neutral His10 imidazole (*7*, *12*, *13*); His10 is also absolutely conserved in all Nox sequences. A major mechanistic difference in the oxidative half-reactions of Npx and Nox is based on the fact that O_2 must be activated by the reduced flavin of Nox (*14*) to yield the singlet peroxide species (*15*), prior to its suspected reaction with Cys42-S^-. The intermediate formation of a C(4a)-peroxyflavin has been considered in one mechanistic proposal for Nox (*16*), but this idea has not been tested by rapid-reaction techniques. Nonetheless, earlier studies of Nox reconstituted with 1-deaza-, 2-thio-, and 4-thio-FAD analogues (*16*) indicated

† This work was supported by National Institutes of Health Grant GM-35394.

* To whom correspondence should be addressed at Department of Biochemistry, Wake Forest University Medical Center, Medical Center Boulevard, Winston-Salem, NC 27157. Telephone: (336) 716-3914. Fax: (336) 716-7671. URL: http://invader.bgsm.wfu.edu/.

[1] Abbreviations: Nox, NADH oxidase; Cys-SOH, cysteine-sulfenic acid; Npx, NADH peroxidase; PHBH, *p*-hydroxybenzoate hydroxylase; HRP, horseradish peroxidase; E, oxidized enzyme; EH_2, two-electron-reduced (FAD, Cys42-SH) enzyme; FADHOOH, C(4a)-peroxyflavin; GR, glutathione reductase.

[2] D. Parsonage, T. C. Mallett, and A. Claiborne, unpublished results.

[3] J.-R. Garel, personal communication.

S0006-2960(98)00363-8 CCC: $15.00
Published on Web 05/27/1998

that the detailed mechanism of oxygen activation differed to some extent from that of *p*-hydroxybenzoate hydroxylase (PHBH; *17*). Modeling studies (*16*) with a C(4a)-peroxyflavin analogue, using the crystal structure for the NADH complex of Npx, demonstrated that the enantiomeric form of the peroxyflavin opposite of that stabilized in PHBH would be required for reaction with Cys42-S^- in the Nox·NAD^+ complex.

A logical mechanism for reduction of this or any other peroxide intermediate would involve, in accordance with the Npx mechanism, nucleophilic attack by Cys42-S^- on peroxide oxygen. As was observed with Npx mutants lacking Cys42 (*12*), replacement of the active-site Cys in Nox should have several effects, including the elimination of the nonflavin redox center as determined in reductive titrations. In addition, such a mutant should prove very useful in studying the oxidative half-reaction, since some kinetic stabilization might be expected for a peroxyflavin intermediate. In this report, we present the initial characterization of the *E. faecalis* Nox C42S mutant; in addition, we present a detailed analysis of the oxidative half-reaction for this mutant. Our results provide evidence for a C(4a)-peroxyflavin intermediate in this reaction and also indicate that a protein conformational or chemical change within the asymmetric, half-reduced Nox dimer is rate-limiting with respect to both reoxidation and turnover.

EXPERIMENTAL PROCEDURES

Materials. NADH, NAD^+, and NADPH were purchased from Boehringer Mannheim; HRP (type VI) was from Sigma, and catalase (bovine liver) was from Calbiochem. Sodium azide was purchased from Fisher; all other chemicals, as purchased from sources described previously (*13*, *16*), were of the best grades available. Expression and purification of both recombinant wild-type *E. faecalis* NADH oxidase and the C42S mutant will be described in a separate communication.[4]

Enzyme Assays and Static Titrations. Spectrophotometric assays of NADH oxidation followed the protocol described previously (*1*), as did oxygen consumption measurements (*16*), except that a standard buffer of 50 mM potassium phosphate (pH 7.0) and 0.5 mM EDTA was used. The same buffer condition was used for all static titrations and stopped-flow experiments, unless otherwise noted. Spectral titrations were carried out with a Hewlett-Packard model 8452A single-beam diode-array spectrophotometer, and fluorescence measurements were made with an SLM Aminco-Bowman Series 2 spectrofluorimeter. Procedures for anaerobiosis have been described (*12*).

Stopped-Flow Kinetics. All rapid-reaction analyses were carried out with the Applied Photophysics DX.17MV stopped-flow spectrophotometer (*12*, *13*), which has been upgraded to include the Applied Photophysics photodiode-array detector. The stopped-flow system was prepared for anaerobic work either as previously described (*12*) or with a newer protocol. A dithionite solution [about 10 mM, in 20 mM Tris sulfate (pH 8.5)] was introduced into both the drive syringes and the mixing chamber; after this overnight scrubbing is completed (at 25 °C), the system is flushed extensively with anaerobic buffer just prior to being used. In addition, solid dithionite (10 g) is added to the circulating liquid [6.6 L of 20 mM Tris-HCl (pH 8.5) and 10% ethanol] in the thermostated water bath just prior to the experiment; the bath is maintained at 5 °C and is continually purged with nitrogen. The contents of the enzyme tonometer and the glass syringes containing buffer were prepared for anaerobic work as previously described (*12*).

When NAD^+ was added to dithionite-reduced C42S Nox, the formation of an NAD^+−sulfite adduct similar to that described by Pfleiderer et al. (*18*) was observed. This adduct was recognized by its near-UV absorbance maximum of about 320 nm, similar to that reported for the NAD^+−cyanide complex (*19*). The presence of this adduct had no effect on either the number of intermediates or the observed rate constants for the oxidative half-reaction with the reduced enzyme·NAD^+ complex; therefore, the fluorescence stopped-flow analyses (where the excitation wavelength range did not go below 340 nm) and the H_2O_2 formation measurements (at 498 nm) were carried out with the dithionite-reduced enzyme·NAD^+ complex, prepared as described below. For all experiments in which the absorbance of the reduced enzyme·NAD^+ complex was monitored directly on reoxidation, however, the complex was prepared in the absence of dithionite. In both cases, the oxidized C42S Nox was taken in a tonometer fitted with a sidearm cuvette (*12*, *20*); after the contents were made anaerobic, the enzyme was titrated with reductant (dithionite or NADPH) from an attached syringe. Stoichiometric reduction was observed with either reductant, as monitored spectrally in the sidearm cuvette. When dithionite was used for reduction, the E-$FADH_2$·NAD^+ complex was prepared by tipping excess NAD^+ (generally a final concentration of 0.16−0.5 mM) from the extension on the sidearm cuvette. When NADPH was used, the reductant syringe was exchanged for one containing anaerobic NAD^+, and formation of the E-$FADH_2$·NAD^+ complex was monitored at 725 nm; these titrations generally required 3.0−3.8 equiv of NAD^+ per $FADH_2$ for completion. $NADP^+$ does not bind the reduced enzyme at these concentrations (NADPH reduction gives no increase in long-wavelength absorbance); there is no interference with NAD^+ binding under these conditions. Free reduced enzyme was prepared for stopped-flow experiments by dithionite titration under similar conditions.

Dissolved oxygen solutions for stopped-flow work were prepared by bubbling buffer in glass syringes (Popper & Sons, New Hyde Park, NY) with either atmospheric or 100% oxygen and either at 25 °C or on ice. The dissolved O_2 concentrations after equilibration with 100% oxygen on ice and at 25 °C are 1.9 (*21*) and 1.3 mM (*16*), respectively. Reoxidation kinetics could therefore be measured at final dissolved O_2 concentrations of 0.13, 0.19, 0.65, and 0.95 mM. Stopped-flow measurements of H_2O_2 formation followed the protocol reported by Powlowski et al. (*22*). The dithionite-reduced E-$FADH_2$·NAD^+ complex (31.4 μM enzyme and 0.16 mM NAD^+ before mixing) was reacted with a solution of HRP (60.2 μM before mixing) containing 0.16 mM NAD^+ and 1.3 mM O_2. Control experiments substituting 30 μM H_2O_2 for the reduced enzyme, in the presence and absence of NAD^+, led to monophasic conversion of HRP → HRP−compound I at 213 s^{-1} (pH 7.0, 5 °C). The reaction was monitored at 498 nm, which is

[4] T. C. Mallett, D. Parsonage, and A. Claiborne, manuscript in preparation.

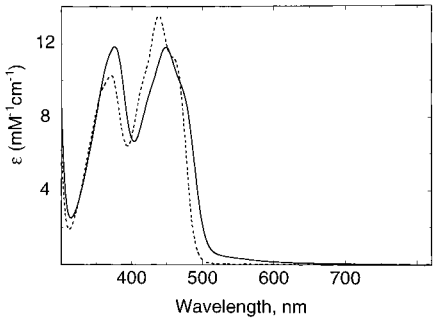

FIGURE 1: Comparison of the visible absorption spectrum of the wild-type Nox E/EH_2 form (—) with that of the C42S mutant enzyme (- -). Spectra shown represent the proteins in 50 mM potassium phosphate (pH 7.0) and 0.5 mM EDTA at 23 °C.

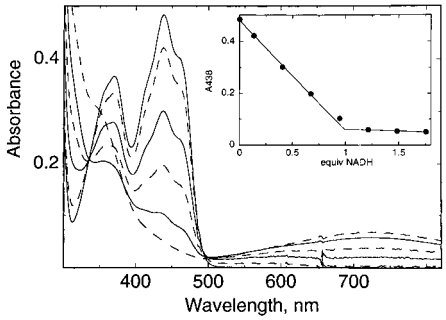

FIGURE 2: Anaerobic titration of C42S Nox with NADH. The anaerobic cuvette contained 1.0 mL of 35.9 μM enzyme (FAD) in the pH 7.0 phosphate buffer. Spectra shown in order of decreasing A_{438} correspond to oxidized enzyme (—) and enzyme after addition of 0.14 (- -), 0.41 (—), 0.68 (- -), 0.95 (—), and 1.76 (- -) equiv of NADH/FAD. The inset shows the absorbance change at 438 nm vs added NADH. The end point corresponds to 0.98 equiv of NADH/FAD. The oxygen-scrubbing system consisting of protocatechuate dioxygenase and protocatechuic acid (*23*) was added anaerobically prior to the titration.

isosbestic for the C42S Nox E-$FADH_2$·NAD^+ and E-FAD species, and the amplitude of the decrease in A_{498} from the control measurement was taken to quantitate H_2O_2 formation by the reduced enzyme.

Reoxidation kinetics were measured at final enzyme concentrations of 10−51 μM and at primary wavelengths of 390 and 438 nm. Reoxidation of the reduced enzyme·NAD^+ complex was also measured at 660 nm. Initial estimates of rate constants and amplitudes were derived from either single- or multiple-exponential fits to these single-wavelength data sets; generally, four independent measurements for each reaction were averaged per data set. This analysis was carried out with the Applied Photophysics DX.17MV and later with SX.18MV software (*20*). Additional global analysis of single-wavelength data from both individual and multiple data sets (for example, in analyzing the excitation wavelength dependency for fluorescence data) was performed with Applied Photophysics Pro-Kineticist (Pro-K) software, which can apply the Marquardt−Levenberg algorithm to simultaneously fit nonlinear rates for all measured wavelengths. The experimental setup for diode-array data acquisition was similar, though at a higher enzyme concentration of 51 μM (after mixing); 100 absorbance spectra were collected over the range of 320−1000 nm, in a logarithmic time base from 1.28 ms to 10 s. The minimum time interval between spectral acquisitions was 2.56 ms. Diode-array data sets were analyzed with Pro-K global analysis software as described in Results; intermediate spectra were calculated by linear regression of the concentration−time curves to the original data set.

RESULTS

Spectral and Redox Properties. Figure 1 gives the visible absorption spectra of the Nox C42S mutant (λ_{max} = 369 and 438 nm; ϵ_{438} = 13 500 M^{-1} cm^{-1}) and the recombinant wild-type Nox as purified (λ_{max} = 376 and 448 nm, and ϵ_{444} = 11 600 M^{-1} cm^{-1} for the E/EH_2 form; *2*). The absorbance ratios at 280 and 450 nm for the purified enzymes are 5.2 and 6.8, respectively. The spectrum of wild-type Nox clearly shows the 535 nm absorbance band attributed to the weak charge-transfer interaction between the EH_2 thiolate (Cys42-S^-) and FAD (*1*, *2*). The C42S mutant spectrum has no absorbance beyond 510 nm, nor is there evidence for any EH_2-like spectral feature in either redox form of the mutant, demonstrating that replacement of Cys42 eliminates the EH_2 charge-transfer interaction. The hyperchromic blue shift in the visible absorbance maximum of the C42S mutant is similar to that observed when Cys42 in the closely related Npx is replaced by Ser (*12*). Another spectroscopic property shared with the Npx C42S mutant is the increased flavin fluorescence which results on Cys42 → Ser substitution. The fluorescence quantum yield for C42S Nox (λ_{max}^{EX} = 438 nm, λ_{max}^{EM} = 520 nm) is 37% of that for free FAD at pH 7.0; this represents an increase of 5-fold over the fluorescence of the wild-type Nox E/EH_2 form. The diminished fluorescence of the wild-type enzyme relative to that of the C42S mutant may be attributed to quenching modes involving Cys42 in both its sulfenic acid (Cys42-SOH) and thiolate (Cys42-S^-) forms.

Reductive titrations of oxidized wild-type Nox (E form) consistently yield stoichiometries of 1.5−1.7 equiv of reductant per FAD (*1*, *2*, *16*). Previous work from this laboratory led to the proposal that the two Cys42-SOH redox centers of the dimeric wild-type Nox are not equivalent (*2*). C42S Nox lacks the proposed sulfenic acid redox center yet retains one tightly bound FAD per subunit. NADH titration of the mutant oxidase leads to direct flavin reduction with 1 equiv of NADH (Figure 2). A small amount of neutral blue semiquinone is observed spectrally (500−650 nm) with the first addition of NADH (total of 0.14 equiv), but an even longer-wavelength band centered at 725 nm begins to predominate at this stage, due to the E-$FADH_2$·NAD^+ charge-transfer interaction. Similar $FADH_2$ → NAD^+ charge-transfer complexes are observed on NADH reductions of both oxidized wild-type Nox (*2*) and the Npx C42S mutant (*12*). The stoichiometric reduction of C42S Nox by NADH is consistent with the elimination of the non-flavin redox center in the mutant.

Catalytic Properties. Standard Nox assays with the C42S mutant at pH 7.0 and 25 °C consistently give specific activity values of 16−20 units/mg; recombinant wild-type Nox has a specific activity of 570 units/mg under the same conditions. In earlier reports from this laboratory, the specific activity of the wild-type Nox purified from *E. faecalis* was reported to be 340 units/mg (*2*); in some enzyme preparations, however, a very labile, high-specific activity (600−700 units/mg) form of the enterococcal enzyme was observed. A method has now been developed which consistently provides

the high-specific activity (560−580 units/mg) form of recombinant wild-type Nox, and a full description of the preparation and properties of the recombinant enzyme will be reported in a separate communication.[4] Considering that in the oxidized wild-type enzyme the sulfenic acid derivative of Cys42 (Cys42-SOH) has been proposed to provide the essential second redox center (*1*, *14*), which participates with the flavin in the overall four-electron reduction of $O_2 \rightarrow 2H_2O$, we also examined the NADH:O_2 reaction stoichiometry of C42S Nox. In a spectrophotometric assay, a catalytic amount (13.4 nM) of the enzyme was incubated with 37 μM NADH in air-saturated (0.26 mM O_2) buffer at 25 °C. NADH oxidation was followed to completion, and the amount of H_2O_2 formed in the reaction mixture was quantitated by the addition of HRP (the initial Nox assay mixture also contained 0.21 mM *o*-dianisidine). Oxidation of 37 μM NADH led to the formation of 1.05 equiv of H_2O_2, demonstrating that H_2O_2 production during turnover by C42S Nox was stoichiometric with NADH oxidation. This result was confirmed in measurements with an oxygen electrode; assays at 0.2 mM NADH led to the stoichiometric consumption of O_2, and subsequent addition of catalase ($2H_2O_2 \rightarrow O_2 + 2H_2O$) restored 52% of the O_2 originally consumed. Mutation of Cys42 → Ser in the enterococcal NADH oxidase, eliminating the Cys42-SOH redox center, thus alters the reaction stoichiometry:

Scheme 1

Wild-type Nox	$2NADH + 2H^+ + O_2 \rightarrow 2NAD^+ + 2H_2O$
C42S Nox	$NADH + H^+ + O_2 \rightarrow NAD^+ + H_2O_2$

Initial velocity studies were carried out in the stopped-flow spectrophotometer varying both [NADH] and [O_2] to determine the turnover number for C42S Nox (k_{cat} = 2.3 s^{-1} at pH 7.0 and 5 °C). Enzyme-monitored turnover analysis of the C42S Nox reaction gave a nearly identical value for k_{cat} (2.2 s^{-1}); in addition, the spectral properties of the enzyme during steady-state turnover are consistent with the participation of a reduced enzyme·NAD^+ complex in the catalytic cycle, since a largely reduced species with long-wavelength (660 nm) absorbance predominates in the spectrum of C42S Nox at the steady state. Detailed analyses of the kinetic mechanisms for wild-type and C42S NADH oxidases will be described in a separate communication.[4]

Oxygen Reactivity of the Reduced C42S Nox·NAD$^+$ Complex. The results presented above demonstrate that C42S Nox forms a stable E-$FADH_2$·NAD^+ complex in static titrations (Figure 2) and furthermore indicate that this complex participates in the catalytic reduction of $O_2 \rightarrow H_2O_2$. To investigate the oxidative half-reaction of C42S Nox in more detail, a series of stopped-flow analyses was performed using both single-wavelength and diode-array data acquisition modes. Figure 3 presents the results of stopped-flow analyses for the reaction of 51 μM C42S Nox E-$FADH_2$·NAD^+ complex (final concentration) with 1 mM O_2 in the presence of 0.34 mM free NAD^+ at pH 7.0 and 5 °C. At 438 nm, the increase in absorbance corresponding to reoxidation of E-$FADH_2$ is biphasic with measured rate constants of 34 and 1.8 s^{-1}. The decrease in A_{660}, which represents the loss of the E-$FADH_2$·NAD^+ charge-transfer absorbance, is also biphasic, but the rate constant for the fast phase is 680 s^{-1}; the rate constant for the slow phase (1.9 s^{-1}) matches

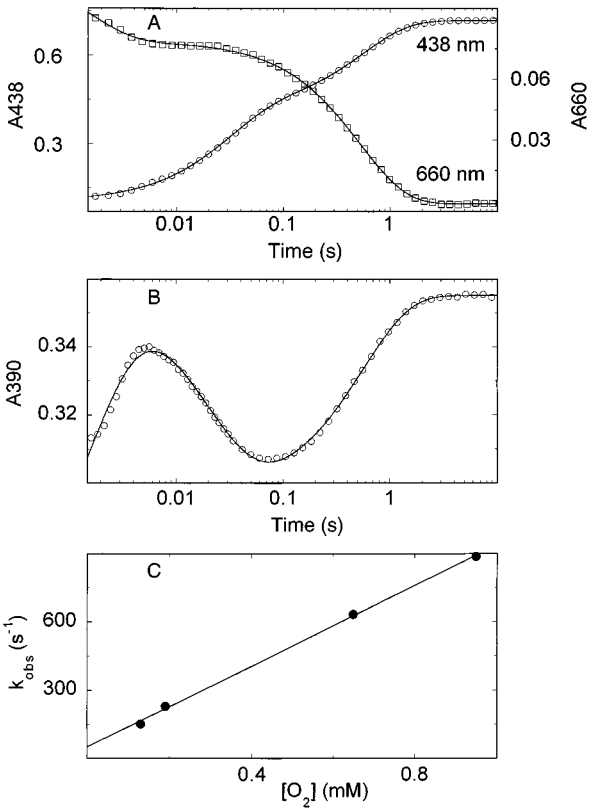

FIGURE 3: Stopped-flow analysis of the reaction of O_2 with the reduced C42S Nox·NAD^+ complex. The complex was prepared anaerobically in a tonometer by sequential titrations of the enzyme with NADPH (1.1 equiv of NADPH/FAD) and NAD^+ (3.8 equiv of NAD^+/$FADH_2$), as described in Experimental Procedures. Complex at 51 μM (after mixing) was reacted with 1 mM O_2 in the pH 7.0 phosphate buffer containing 0.34 mM free NAD^+, in the Applied Photophysics stopped-flow spectrophotometer thermostated at 4.7 °C. (A) The reaction was monitored at 438 (○) and 660 nm (□). (B) The reaction was monitored at 390 nm (○). (C) Direct plot of k_{obs} for the fast phase of reoxidation at 390 nm vs [O_2]. These data were obtained in an experiment similar to that described in panel B in which the NADPH-reduced enzyme·NAD^+ complex (14.8 μM after mixing; prepared as described above) was reacted with NAD^+ solutions (0.09 mM) containing different dissolved O_2 concentrations. The temperature was 5.5 °C.

that of 1.8 s^{-1} measured at 438 nm. As shown in Figure 3, all three phases are observed at 390 nm. The fast phase consists of an increase in A_{390} (k_{obs} = 570 s^{-1}) and is followed by a decrease (k_{obs} = 46 s^{-1}); the rate constant for the third phase (1.7 s^{-1}) is consistent with the limiting rate constants measured at 438 and 660 nm. Analysis of the [O_2] dependencies for the three rate constants demonstrates that the two slower phases are [O_2]-independent; only the fast phase is [O_2]-dependent (Figure 3), with a second-order rate constant of 8.5 × 10^5 M^{-1} s^{-1} at pH 7.0 and 5 °C. The second-order plot has a finite non-zero intercept corresponding to a first-order rate constant of 56 s^{-1} for dissociation of the complex. A minimal kinetic scheme which accounts for these data is as follows:

Scheme 2

$$\text{E-FADH}_2\cdot\text{NAD}^+ + O_2 \underset{56\ s^{-1}}{\overset{8.5 \times 10^5\ M^{-1}s^{-1}}{\rightleftharpoons}} \text{B}$$

$$\text{B} \xrightarrow{34\text{-}46\ s^{-1}} \text{C}$$

$$\text{C} \xrightarrow{1.7\text{-}1.9\ s^{-1}} \text{E-FAD} + H_2O_2 + NAD^+$$

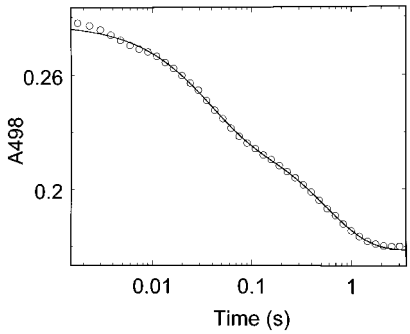

FIGURE 4: Stopped-flow analysis of H_2O_2 formation during reoxidation of the reduced enzyme·NAD^+ complex. The complex was prepared by tipping 0.16 mM NAD^+ to 30.4 μM dithionite-reduced C42S Nox in a tonometer, as described in Experimental Procedures. The complex was then reacted with a buffered solution containing 0.16 mM NAD^+, 1.3 mM O_2 (before mixing), and 60 μM HRP, and the formation of HRP−compound I was measured at 498 nm. The temperature was 5.3 °C.

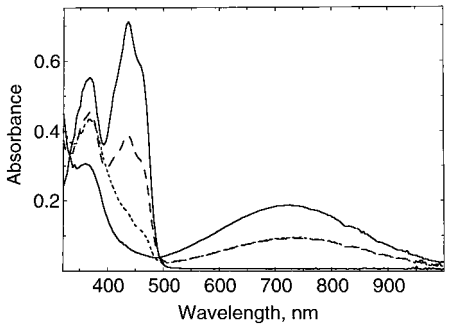

FIGURE 5: Stopped-flow diode-array analysis of the reoxidation of the reduced enzyme·NAD^+ complex. Experimental conditions are identical to those given in Figure 3A,B, except that spectral data were acquired with the photodiode-array detector interfaced to the Applied Photophysics stopped-flow instrument. Spectra correspond to the reduced complex (—, after mixing with anaerobic buffer), the O_2 reaction mixture at 6.4 (- -) and 50 ms (— —), and the final reoxidized enzyme 5 s after mixing (—). The temperature was 4.7 °C.

The initial oxygen reaction is observed at both 390 and 660 nm, but there is almost no fast reaction at 438 nm; the increase in A_{438} proceeds after a lag, as a much slower, $[O_2]$-independent biphasic conversion to E-FAD. The $[O_2]$-independent conversion of B → C is observed at both 390 and 438 nm, but there is essentially no observable reaction at 34−46 s^{-1} at 660 nm; this indicates that A_{660} values for intermediates B and C are the same, i.e., that this is an isosbestic point. The conversion of C → E-FAD can be measured at all three wavelengths, and the rate constant of 1.7−1.9 s^{-1} is very similar to the turnover number (2.2−2.3 s^{-1}) determined for C42S Nox at pH 7.0 and 5 °C, indicating that this process is largely rate-limiting in catalysis as well.

Kinetics of H_2O_2 Formation. An obvious question raised by the kinetic scheme presented above concerns the identity of the step(s) involving formation of H_2O_2 in the oxidative half-reaction, and this was addressed by using horseradish peroxidase (HRP). In studies of the flavoprotein anthranilate hydroxylase (*22*), the rapid H_2O_2-dependent conversion of HRP to HRP−compound I (and II) was monitored during reoxidation of the free reduced flavoprotein to demonstrate that H_2O_2 formation corresponded to the fast phase in enzyme reoxidation. The reoxidation of C42S Nox E-$FADH_2$·NAD^+ (16 μM final concentration) was then analyzed in the presence of 30 μM HRP; the conversion of HRP → HRP−compound I was measured at 498 nm, a wavelength which is isosbestic for E-$FADH_2$·NAD^+ and E-FAD. Surprisingly, the decrease in A_{498} in this experiment is biphasic (Figure 4), with rate constants of 29 and 1.8 s^{-1}, respectively. Furthermore, each phase accounted for nearly one-half of the total ΔA_{498} (48 and 52%, respectively). The total ΔA_{498} was essentially identical to that observed when 15 μM H_2O_2 (final concentration) was reacted with 30 μM HRP at pH 7.0 and 5 °C (k_{obs} = 213 s^{-1} for the monophasic reaction at 498 nm), and the rate constants of 29 and 1.8 s^{-1} measured in the presence of C42S Nox are consistent with those presented in Scheme 2 for the sequential conversion of intermediate B → C and of intermediate C → E-FAD. On the basis of this analysis, Scheme 2 can be modified to account for the biphasic formation of H_2O_2:

Scheme 3

$$\text{E-FADH}_2\cdot\text{NAD}^+ + \text{O}_2 \underset{56\ \text{s}^{-1}}{\overset{8.5\times10^5\ \text{M}^{-1}\text{s}^{-1}}{\rightleftharpoons}} \text{B}$$

$$\text{B} \xrightarrow{34\text{-}46\ \text{s}^{-1}} \text{C} + 0.5\ \text{H}_2\text{O}_2$$

$$\text{C} \xrightarrow{1.7\text{-}1.9\ \text{s}^{-1}} \text{E-FAD} + 0.5\ \text{H}_2\text{O}_2\ (+\ \text{NAD}^+)$$

The observation that both steps in the conversion of B → E-FAD involve the formation of 0.5 equiv of H_2O_2 per FAD is entirely consistent with the observation that the slow phase (k_{obs} = 1.7−1.9 s^{-1}) measured at 438 nm during reoxidation of C42S Nox E-$FADH_2$·NAD^+ accounts for about one-half of the total ΔA_{438}. This implies, in combination with the HRP analysis, that conversion of B → C accounts for one-half of the E-$FADH_2$·NAD^+ → E-FAD conversion, as does the conversion of C → E-FAD.

Diode-Array Analysis. The observation that intermediate B is formed in the $[O_2]$-dependent reaction and decays in two steps to release 1 equiv of H_2O_2 per FAD indicates that it is an oxygenated flavin species. The A_{660} trace described in Figure 3 also indicates, however, that this intermediate retains significant long-wavelength absorbance characteristic of the E-$FADH_2$·NAD^+ complex. To examine the spectral characteristics of intermediates B and C, the reaction of the C42S Nox E-$FADH_2$·NAD^+ complex with O_2 was analyzed under conditions identical to those described for the single-wavelength measurements, but using photodiode-array detection. Figure 5 gives spectra of the E-$FADH_2$·NAD^+ complex at 5 °C and of the reaction mixture 6.4 ms, 50 ms, and 5 s after mixing in the stopped-flow spectrophotometer. The spectrum of the reduced enzyme was recorded on mixing with an equal volume of anaerobic buffer, in the presence of excess NAD^+; the enhanced long-wavelength absorbance (λ_{max} = 725 nm; ϵ_{725} = 3550 M^{-1} cm^{-1}) relative to that given in Figure 2 is due to the marked temperature dependence of this charge-transfer feature (*2*). From comparison of the difference spectra (data not shown) obtained by subtracting the reduced enzyme spectrum from each of those presented above, it is apparent that the reaction mixture at 6.4 ms is characterized by a rather broad increase in absorbance over the range of 340−480 nm. The increase in A_{438} is equivalent to about 16−17% E-FAD formation, but the ΔA_{max} is about 370−395 nm. At 725 nm, the 6.4 ms spectrum has lost 51%

of the E-$FADH_2$·NAD^+ charge-transfer absorbance. Inspection of the 50 ms spectrum over the range of 340−490 nm shows that it is consistent with the formation of E-FAD; at 438 nm, the ΔA is exactly 51% of that measured at the end of the reaction. In sharp contrast, there is essentially no ΔA between the 6.4 and 50 ms spectra over the range of 490−1000 nm; the 50 ms spectrum retains exactly 51% of the original E-$FADH_2$·NAD^+ charge-transfer absorbance. Between 50 ms and 5 s, the full absorbance of E-FAD returns, and the remaining long-wavelength absorbance is lost. In the difference spectra, the 50 ms and 5 s plots share an isosbestic point at about 493 nm, similar to the isosbestic point at 498 nm for the C42S Nox E-FAD and E-$FADH_2$·NAD^+ forms.

Using the entire 1.28 ms to 10 s diode-array data set (wavelength range of 320−1000 nm; 100 spectra acquired in logarithmic time base), a series of three exponentials was fit with the global analysis software. Initial estimates of rate constants for the three phases were taken from the single-wavelength analyses in the same experiment (Figure 3); the model was then fit to the data (variance = 6.2×10^{-5}) iteratively using the Marquardt−Levenberg algorithm (see Experimental Procedures). The rate constants obtained are consistent with those given in Scheme 3 and provide for the following reaction sequence, where the [O_2]-dependent formation of intermediate B is described with a pseudo-first-order rate constant:

Scheme 4

$$\text{E-FADH}_2\cdot\text{NAD}^+ + \text{O}_2 \xrightarrow{680\ s^{-1}} \text{B}$$

$$\text{B} \xrightarrow{35\ s^{-1}} \text{C} + 0.5\ \text{H}_2\text{O}_2$$

$$\text{C} \xrightarrow{2\ s^{-1}} \text{E-FAD} + 0.5\ \text{H}_2\text{O}_2\ (+\ \text{NAD}^+)$$

The concentration−time curves for this scheme indicate that intermediates B and C reach maximal levels corresponding to 83 and 85%, respectively, of the total enzyme at 6.4 and 90 ms. The 50 ms spectrum shown in Figure 5 consists of 77% intermediate C, 19% intermediate B, and about 5% E-FAD, as derived from the model. The global fit allows for the calculation of the absorbance spectra of intermediates B and C; this is based on the kinetic model presented in Scheme 4 and on the measured spectral parameters for both E-$FADH_2$·NAD^+ (species A) and E-FAD (species D). Figure 6 presents the spectra measured for E-$FADH_2$·NAD^+ and E-FAD along with the calculated spectra for intermediates B and C. The reduced C42S Nox·NAD^+ complex has absorbance maxima at 359 and 725 nm, with ϵ values of 5820 and 3550 M^{-1} cm^{-1}, respectively. Intermediate B appears on reaction of O_2 with the reduced enzyme; this species has absorbance maxima at 368 and 725 nm (ϵ = 8220 and 1750 M^{-1} cm^{-1}, respectively), with a low-extinction shoulder at ~460 nm. The conversion of intermediate B → C leads to the appearance of an oxidized enzyme absorbance maximum at 438 nm (ϵ = 8100 M^{-1} cm^{-1}), but only small absorbance changes occur from 340 to 400 nm. The calculated spectra for intermediates B and C are identical over the range of 500−1000 nm. The final oxidized enzyme (E-FAD) has no absorbance beyond 510 nm, and the absorbance maxima of 368 and 438 nm correspond to ϵ values of 10 490 and 13 500 M^{-1} cm^{-1}, respectively.

Intermediate B Contains a C(4a)-Peroxyflavin Component. On the basis of the observation that its rate of formation is dependent on [O_2] and its spectral characteristics in the 340−490 nm region, it is tempting to assign the structure of an FAD C(4a)-hydroperoxide to intermediate B. The spectrum of intermediate B in the near-UV region (λ_{max} = 368 nm, ϵ = 8.2 mM^{-1} cm^{-1}) can be compared with those of the FAD C(4a)-hydroperoxides in PHBH (λ_{max} = 382−385 nm, ϵ = 8.7−9.7 mM^{-1} cm^{-1}; *24*) in the presence of 0.1 M azide (with and without *p*-hydroxybenzoate), in the microsomal FAD-containing monooxygenase (λ_{max} = 366 nm, ϵ = 10.8 mM^{-1} cm^{-1}; *25*) in the presence of $NADP^+$, and in phenol hydroxylase (λ_{max} = 385 nm, ϵ = 10.5 mM^{-1} cm^{-1}; *26*) in the presence of thiophenol and 0.25 M KCl. Model studies (*27*) with 5-ethyl-4a-peroxylumiflavin in acetonitrile give a λ_{max} of 367 nm with an ϵ of 9.4 mM^{-1} cm^{-1}, and the 5-ethyl-4a-hydroxy-FAD PHBH complex with *p*-hydroxybenzoate has a λ_{max} of 368 nm with an ϵ of 8.4 mM^{-1} cm^{-1}. On the other hand, the charge-transfer absorbance centered at 725 nm in intermediate B is unprecedented among the C(4a)-peroxyflavin intermediates of other monooxygenases, including the FAD C(4a)-hydroperoxide·$NADP^+$ complex of the microsomal monooxygenase (*25*), which exhibits no absorbance beyond 500 nm. Another question regarding the assignment of the peroxyflavin structure to intermediate B concerns the biphasic release of H_2O_2, although similar behavior was seen on reoxidation of free, reduced PHBH in the presence of azide (*24*). An alternative interpretation which could answer both of these questions regarding the structure of intermediate B is that the oxygen reactivities at the two $FADH_2$ per dimer are not equivalent; if one E-$FADH_2$·NAD^+ per dimer remains in intermediate B, this would account for both the long-wavelength absorbance component (ϵ_{725} is 49% of that for the reduced enzyme·NAD^+ complex) and the biphasic reoxidation kinetics (B → C → E-FAD; where ϵ_{438} for intermediate C is 60% of that for E-FAD) for species B. The observation that the long-wavelength absorbance component is unchanged in intermediate C, which is converted to E-FAD at 2 s^{-1} as 0.5 equiv of H_2O_2 per FAD is formed, suggests that one $FADH_2$·NAD^+ per dimer might remain with this species as well.

To address this possibility, the spectral properties of intermediates B and C were analyzed in more detail, with two alternative descriptions of these species in mind. In one case, both $FADH_2$·NAD^+ species react rapidly with O_2 to yield peroxyflavin intermediates; the long-wavelength ab-

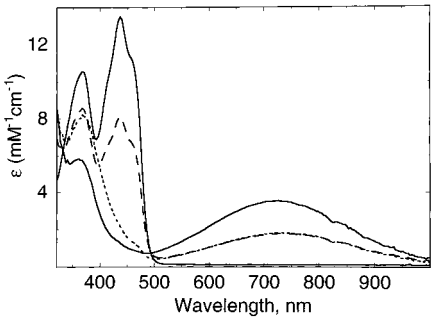

FIGURE 6: Calculated absorption spectra for intermediates B and C. The entire 10 s, 100-spectrum data set from the diode-array experiment described in Figure 5 was analyzed as described in Experimental Procedures and Results, for the three-step model presented in Scheme 4. The spectra shown for the starting reduced enzyme·NAD^+ complex (—) and fully oxidized enzyme (—) are taken from Figure 5. Additional spectra shown were calculated for intermediate B (- -) and intermediate C (— —).

sorbance must involve some type of charge-transfer interaction between C(4a)-FADHOOH (perhaps as the hydroperoxide anion; *28*) and NAD^+. Some conformational or chemical distinction between the two FADHOOH per dimer allows for the biphasic formation of H_2O_2:

Scheme 5

$$\frac{FADH_2 \cdot NAD^+}{FADH_2 \cdot NAD^+} + 2O_2 \xrightarrow{680\ s^{-1}} \frac{FADHOOH}{FADHOOH \rightarrow NAD^+} (+ NAD^+)$$

"B"

$$\frac{FADHOOH}{FADHOOH \rightarrow NAD^+} \xrightarrow{35\ s^{-1}} \frac{FAD}{FADHOOH \rightarrow NAD^+} + H_2O_2$$

"C"

$$\frac{FAD}{FADHOOH \rightarrow NAD^+} \xrightarrow{2\ s^{-1}} \frac{FAD}{FAD} + NAD^+ + H_2O_2$$

Over the range of 340−500 nm, the calculated spectrum of intermediate C should compare favorably with the sum of 50% B and 50% E-FAD; in fact, this is not the case. The shape of the addition spectrum is quite different from the calculated spectrum, especially in the 340−425 nm region; the $\epsilon_{366}/\epsilon_{438}$ ratio is 14% higher, and the individual ϵ_{366} and ϵ_{395} values are 10−18% higher for the addition spectrum. So we conclude that this description for intermediates B and C is not correct. The alternative description, in which one $FADH_2 \cdot NAD^+$ per dimer remains in each intermediate, can be represented as follows:

Scheme 6

$$\frac{FADH_2 \cdot NAD^+}{FADH_2 \cdot NAD^+} + O_2 \xrightarrow{680\ s^{-1}} \frac{FADHOOH}{FADH_2 \cdot NAD^+} (+ NAD^+)$$

"B"

$$\frac{FADHOOH}{FADH_2 \cdot NAD^+} \xrightarrow{35\ s^{-1}} \frac{FAD}{FADH_2 \cdot NAD^+} + H_2O_2$$

"C"

$$\frac{FAD}{FADH_2 \cdot NAD^+} \xrightarrow{2\ s^{-1}} \frac{FAD}{(FADH_2 \cdot NAD^+)^*}$$

$$\frac{FAD}{(FADH_2 \cdot NAD^+)^*} + O_2 \xrightarrow{>>2\ s^{-1}} \frac{FAD}{FAD} + NAD^+ + H_2O_2$$

The calculated spectrum for intermediate C should compare very favorably with the sum of 50% E-$FADH_2 \cdot NAD^+$ and 50% E-FAD, and the difference obtained by subtracting 50% E-$FADH_2 \cdot NAD^+$ from the calculated spectrum for intermediate B should give the spectrum for the C(4a)-FADHOOH species. This addition spectrum gives a much more favorable comparison than that described above in terms of the shape of the spectrum between 340 and 500 nm, the $\epsilon_{366}/\epsilon_{438}$ ratio (1.1 compared to 1.05 for the calculated spectrum), the individual ϵ_{366} and ϵ_{438} values (within 5 and 9% of the values from the calculated spectrum, respectively), and the match between long-wavelength spectral components (500−1000 nm). The minor differences between this addition spectrum and the calculated spectrum disappear almost entirely if a component equivalent to only 5−6% of the final E-FAD spectrum is added to the addition spectrum itself (Figure 7). In addition, Figure 7 gives the spectrum for the C(4a)-FADHOOH component of intermediate B determined by subtraction as described above. The absorbance maximum of 372 nm ($\epsilon = 10.7\ mM^{-1}\ cm^{-1}$) compares very favorably with those for both enzymic and model peroxyflavins as described previously (*24*−*28*). We conclude from these data that the reoxidation of the reduced C42S Nox·NAD^+ complex proceeds through two intermediates, each of which includes one E-$FADH_2 \cdot NAD^+$ per dimer. The oxygen

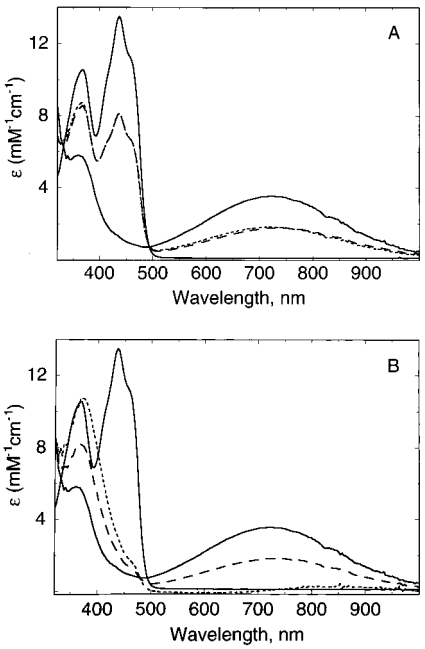

FIGURE 7: Spectral deconvolution for intermediates B and C. (A) Spectra corresponding to the starting reduced complex (—), fully oxidized enzyme (—), and intermediate C (— —) are from Figure 6. Also given is the addition spectrum (- -) obtained by adding 47% of the reduced complex spectrum and 53% of the fully oxidized enzyme spectrum. (B) Spectra corresponding to the starting reduced complex (—), fully oxidized enzyme (—), and intermediate B (— —) are from Figure 6. Also given is the spectrum (- -) obtained by subtracting 50% of the reduced complex spectrum from the intermediate B spectrum and multiplying by 2.

reactivity of this reduced flavin is limited by a conformational or chemical change which occurs once the primary $FADH_2$ has completed its reaction sequence; therefore, the sequential kinetic mechanism presented in Scheme 6 is appropriate. The rate constant for the limiting conformational or chemical change is identical to k_{cat} for the C42S mutant. This also represents, presuming the oxygen reactivity of wild-type Nox proceeds through a similar peroxyflavin intermediate, the first example of such an oxygenated flavin intermediate outside the flavoprotein monooxygenase class (*15*).

Stopped-Flow Fluorescence Analysis. Ghisla et al. (*27*) demonstrated that PHBH reconstituted with 5-ethyl-4a-hydroxy-FAD is 30% as fluorescent as native enzyme, and the presence of bound 6-aminonicotinate enhanced the fluorescence 4-fold. The FAD C(4a)-hydroperoxide observed on reaction of the reduced PHBH·6-hydroxynicotinate complex with O_2, however, is not fluorescent; the absence of fluorescence was attributed to small differences in coenzyme−protein interactions. Maeda-Yorita and Massey (*28*), on the other hand, established the presence of two peroxyflavin forms in the oxygen reaction of the phenol hydroxylase·resorcinol complex; while both forms are fluorescent in the absence of azide, the presence of azide quenched the fluorescence of one species while enhancing the fluorescence of the second FADHOOH form. We analyzed the oxygen reaction of the reduced C42S Nox·NAD^+ complex by fluorescence with two goals in mind. First, we wanted to characterize the fluorescence of the FADHOOH component of intermediate B (Scheme 6). In addition, since the appearance of oxidized flavin is biphasic during reoxidation of E-$FADH_2 \cdot NAD^+$, and since the E-FAD form of

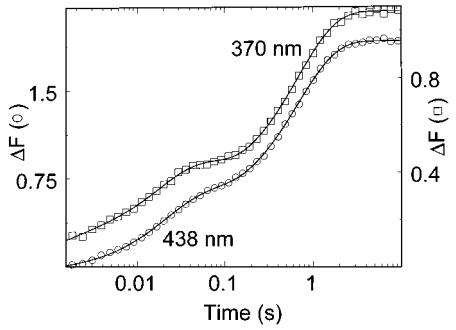

FIGURE 8: Stopped-flow fluorescence analysis of the reoxidation of the reduced C42S Nox·NAD^+ complex. The dithionite-reduced enzyme·NAD^+ complex (20 μM before mixing, with 0.5 mM free NAD^+) was reacted with a buffered solution containing 0.5 mM NAD^+ and 0.38 mM O_2 in the Applied Photophysics stopped-flow instrument. Using an emission cutoff filter which allows transmission of light at wavelengths >475 nm, the reoxidation traces shown correspond to excitation wavelengths of 370 (□) and 438 nm (○). Data were fit to the kinetic model presented in Scheme 7, using the global analysis software. Fluorescent units are arbitrary, and the temperature was 4.5 °C.

C42S Nox is 37% as fluorescent as free FAD, Scheme 6 predicts that intermediate C is about one-half as fluorescent as E-FAD. Figure 8 presents the stopped-flow result obtained when 10 μM E-$FADH_2$·NAD^+ complex (final concentration) is reacted with 0.2 mM O_2 in the presence of 0.5 mM free NAD^+; fluorescence emission data were collected at wavelengths greater than 475 nm (475 nm cutoff filter), with excitation wavelengths varied at 10 nm intervals from 340 to 450 nm. When monitored at $\lambda^{EX} = 438$ nm, the reaction trace is generally similar to that obtained in the absorbance mode at 438 nm; in addition, the $\lambda^{EX} = 370$ nm fluorescence trace gives no evidence for any rapid phase corresponding to the formation of a fluorescent species. From this, we conclude that intermediate B [FADHOOH/$FADH_2$·NAD^+] is nonfluorescent; the peroxyflavin component ($\lambda_{max} = 372$ nm) therefore resembles that seen in the reduced PHBH·6-hydroxynicotinate reaction with O_2 (*27*). The entire stopped-flow fluorescence data set was then used to fit a series of exponentials with the global analysis software. The three-step model presented in Scheme 4, with a pseudo-first-order rate constant of 231 s^{-1} substituted for the oxygen-dependent formation of intermediate B, does not fit the fluorescence data set. The global fit requires four consecutive reactions; three of these rate constants correspond directly to the model derived from the absorbance data, while one intermediate (C_F) is detected only by fluorescence:

Scheme 7

$$\text{E-FADH}_2\cdot\text{NAD}^+ + \text{O}_2 \xrightarrow{231\ s^{-1}} \text{B}$$

$$\text{B} \xrightarrow{38\ s^{-1}} \text{C} + 0.5\ \text{H}_2\text{O}_2$$

$$\text{C} \xrightarrow{28\ s^{-1}} \text{C}_F$$

$$\text{C}_F \xrightarrow{1.5\ s^{-1}} \text{E-FAD} + 0.5\ \text{H}_2\text{O}_2\ (+\ \text{NAD}^+)$$

The oxygen reaction yielding the peroxyflavin component appears as a lag in the development of fluorescence, since intermediate B is nonfluorescent. The second rate constant of 38 s^{-1} is consistent with the [O_2]-independent conversion (35 s^{-1}) of intermediate B → C, as described in Scheme 4. The additional step unique to the fluorescence data corresponds to the formation of intermediate C_F at 28 s^{-1}; this species is less fluorescent than intermediate C when analyzed at excitation wavelengths from 340 to 390 nm. From 400 to 450 nm, the two species exhibit very similar fluorescence intensities of about 30% of that for the final oxidized enzyme (E-FAD). Although the absorbance spectrum calculated for intermediate C (ϵ_{438} = 60% of that for E-FAD) is indistinguishable from that of C_F, the conversion of C_F → E-FAD at 1.5 s^{-1} accounts for 70% of the total fluorescence increase on reoxidation of the reduced enzyme, across the excitation wavelength range investigated. The two major phases of flavin reoxidation measured in absorbance at 438 nm (B → C → E-FAD) do not correspond to exactly equal changes in fluorescence, implying that the FAD component of intermediate C (or C_F) is less fluorescent than the FAD of the fully oxidized enzyme. A possible basis for the fluorescence change as C → C_F could be the release of spectrally silent NAD^+ following H_2O_2 elimination from the FADHOOH component of intermediate B:

Scheme 8

$$\underset{\text{"B"}}{\frac{\text{FADHOOH(NAD}^+\text{)}}{\text{FADH}_2\cdot\text{NAD}^+}} \xrightarrow{35\text{-}38\ s^{-1}} \underset{\text{"C"}}{\frac{\text{FAD(NAD}^+\text{)}}{\text{FADH}_2\cdot\text{NAD}^+}} + \text{H}_2\text{O}_2$$

$$\underset{\text{"C"}}{\frac{\text{FAD(NAD}^+\text{)}}{\text{FADH}_2\cdot\text{NAD}^+}} \xrightarrow{28\ s^{-1}} \underset{\text{"C}_F\text{"}}{\frac{\text{FAD}}{\text{FADH}_2\cdot\text{NAD}^+}} + \text{NAD}^+$$

Oxygen Reactivity of Reduced C42S Nox in the Presence of Azide. Among the FAD-containing monooxygenases, it is generally observed (*24*) that the hydroxylatable substrate, or an effector analogue, kinetically stabilizes the corresponding C(4a)-peroxyflavin which is formed on direct reaction of the reduced enzyme·substrate complex with O_2. Exceptions are found in the microsomal FAD-containing monooxygenase (*25*) and cyclohexanone monooxygenase (*29*), where bound $NADP^+$ stabilizes the peroxyflavin, and in *p*-hydroxyphenylacetate 3-hydroxylase (*30*), where a coupling protein stabilizes the primary oxygenated species. Still, the free reduced enzymes react with O_2 in all cases without directly observable FADHOOH intermediates, although Entsch et al. (*24*) demonstrated that bound azide ion led to stabilization of the PHBH peroxyflavin in a manner somewhat similar to that seen with bound effectors. Azide binds to oxidized forms of both wild-type and C42S Nox; it is a linear mixed-type inhibitor of the wild-type enzyme (*16*) but does not inhibit the mutant in standard NADH oxidation assays. Azide does, however, interfere with the interaction of reduced C42S Nox with NAD^+ in static experiments, thus precluding studies of E-$FADH_2$·NAD^+ reoxidation kinetics in the presence of azide. A complete description of the interaction of azide and chloride ion with both wild-type and C42S Nox will be reported in a separate communication.[4] The reaction of reduced C42S Nox (12.7 μM final concentration) with O_2 was investigated in the presence of 0.1 M azide; reoxidation was followed at 390 and 438 nm and at final O_2 concentrations of 0.13 and 0.65 mM. Simple biphasic reoxidation is observed at both wavelengths (Figure 9); the first phase corresponds to an altered [O_2]-dependent reaction with a second-order rate constant of 2.1×10^4 M^{-1} s^{-1} (a decrease of 40-fold with azide present instead of NAD^+) at pH 7.0 and 5 °C and a first-order rate constant of 5.4 s^{-1} for dissociation of the oxygen complex. Again, as with the reaction of E-$FADH_2$·NAD^+, the final phase of

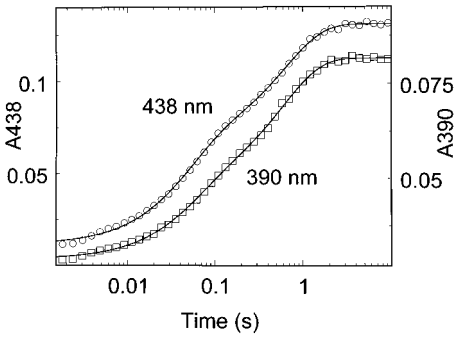

FIGURE 9: Stopped-flow analysis of the reoxidation of reduced C42S Nox in the presence of 0.1 M azide. Dithionite-reduced enzyme (25.4 μM before mixing) was reacted with a buffered solution containing 1.3 mM O_2 and 0.2 M azide. The reaction was monitored in the Applied Photophysics stopped-flow instrument at 390 (□) and 438 nm (○). The temperature was 4.4 °C.

reoxidation corresponds to an $[O_2]$-independent rate constant of 0.8−1.7 s^{-1}. At 438 nm, the slow phase accounts for about one-half (45−54%) of the total absorbance increase. This behavior is similar to that described previously for the conversion of [FAD/$FADH_2$·NAD^+] to E-FAD. The kinetic scheme for reaction with azide present is as follows:

Scheme 9

$$\text{E-FADH}_2(N_3^-) + O_2 \underset{5.4\ s^{-1}}{\overset{2.1 \times 10^4\ M^{-1}s^{-1}}{\rightleftharpoons}} [X]$$

$$[X] \xrightarrow{0.8\text{-}1.7\ s^{-1}} \text{E-FAD} \cdot N_3^-$$

The available data indicate that no peroxyflavin is observed directly in the presence of azide, but it is possible that such a species is formed, decaying rapidly to give the observed intermediate:

Scheme 10

$$\text{E-FADH}_2(N_3^-) + O_2 \underset{5.4\ s^{-1}}{\overset{2.1 \times 10^4\ M^{-1}s^{-1}}{\rightleftharpoons}} \left[\frac{\text{FADHOOH}}{\text{FADH}_2}\right](N_3^-) \xrightarrow{\text{fast}} [X]$$

A similar analysis of the reoxidation of free reduced C42S Nox gives kinetic data consistent with a very small extent of peroxyflavin formation, as shown by a rapid increase (k = 4.3 × 10^5 M^{-1} s^{-1}) in A_{390}. While the observed rate constant is dependent on $[O_2]$, the corresponding ΔA only accounts for ∼20% of the total ΔA_{390} at 0.65 mM O_2. Biphasic reoxidation is also seen at 438 nm, but both rate constants of 12−15 and 0.8−1.8 s^{-1} are independent of $[O_2]$; the latter value is consistent with that for the slow phase (0.9−1.8 s^{-1}) at 390 nm. From the analyses presented above, it can be concluded that (1) azide does not stabilize the peroxyflavin intermediate of C42S Nox and (2) the rate-limiting step in the oxidative half-reaction appears to be independent of the presence of NAD^+. The latter conclusion is consistent with the suggestion (Scheme 6) that a conformational change within the [FAD/$FADH_2$·NAD^+] dimer is limiting (k = 1.7−1.9 s^{-1}) to full reoxidation.

DISCUSSION

NADH oxidase (Nox) and NADH peroxidase (Npx) from *E. faecalis* are members of the glutathione reductase (GR) class of pyridine nucleotide-dependent flavoprotein disulfide reductases (*31*); recent evidence indicates that the *Staphylococcus aureus* coenzyme A disulfide reductase (*32*) is closely related to Nox and Npx as well. The utilization of the Cys-SOH redox center, as demonstrated for Npx and favored strongly for Nox, instead of the redox-active cystine disulfide employed by GR, represents the primary point of contrast between the two peroxide reductases and the GR-like disulfide reductases. Given the homology between Nox and Npx (*6*), the high-resolution crystal structure for Npx (*33*), and the results of earlier analyses of Npx mutants lacking Cys42 and His10 (*12*, *13*), a plausible chemical mechanism for the oxidative half-reaction of Nox involves the sequence

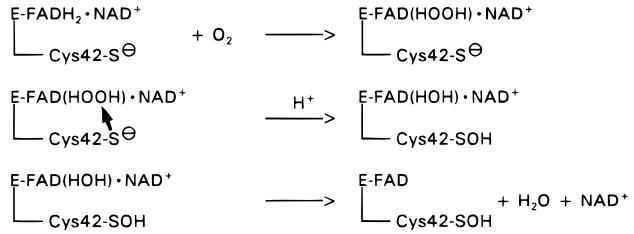

His10, which is absolutely conserved in all Nox sequences, is not an essential acid−base catalyst in Npx (*13*); rather, it functions to stabilize the transition state during the nucleophilic attack of Cys42-S^- on HOOH, through hydrogen-bonding interactions with the peroxide oxygen(s). His10 also serves to stabilize Cys42-SOH in the resting peroxidase, and both functions fit in well with the mechanistic scheme presented for Nox above. A major question raised by the proposed Nox mechanism concerns the possibility that an FAD C(4a)-hydroperoxide intermediate is involved in the Nox catalytic cycle or whether H_2O_2 formed on $FADH_2$ reoxidation is immediately trapped by the peroxidatic Cys42-S^- center. To this end, we have examined the oxidative half-reaction of the Nox C42S mutant in detail.

In contrast with those for wild-type Nox, reductive titrations of the C42S mutant require only 1 equiv of NADH per FAD and lead directly to the $FADH_2$·NAD^+ form of the enzyme. Furthermore, while the C42S mutant does have significant catalytic activity (k_{cat} = 900 min^{-1} at 25 °C), the reaction stoichiometry is changed from the tetravalent reduction of $O_2 \rightarrow 2H_2O$ to NADH + H^+ + $O_2 \rightarrow NAD^+$ + H_2O_2. These results confirm that Cys42, almost certainly in the Cys42-SOH form as proposed, is the non-flavin redox center in wild-type Nox. In addition, these results strongly support the idea that Cys42-S^- in wild-type Nox functions in the further reduction of some two-electron-reduced oxygen intermediate. The oxidative half-reaction for wild-type Nox can be thought to consist of a flavoprotein oxidase (O_2 + $FADH_2 \rightarrow$ ROOH; R ≡ FADH or H) component coupled with a peroxidase (ROOH + Cys42-S^- + $H^+ \rightarrow$ ROH + Cys42-SOH) component; Cys42 is the peroxidatic center, and its elimination leads to the catalytic generation of H_2O_2 by the functioning flavoprotein oxidase center. The spectroscopic properties of C42S Nox confirm that Cys42-S^- is the charge-transfer donor in the two-electron-reduced wild-type enzyme; the enhanced fluorescence of C42S Nox is consistent with that seen when the analogous mutation is introduced in Npx and supports the idea that Cys42-SOH and Cys42-S^- both contribute to the flavin fluorescence quenching modes in Nox and Npx.

The combination of diode-array and single-wavelength stopped-flow analyses of the oxidative half-reaction of C42S

Nox allows for a rather direct interpretation of the sequence of events. To begin, we have shown that, in turnover under [NADH]-limited conditions, the reduced C42S Nox·NAD^+ complex predominates. The $FADH_2$·NAD^+ species as generated in static titrations is extremely stable, even at 1 equiv of NAD^+ per $FADH_2$, suggesting that dissociation of NAD^+ is negligible. For these reasons, we conclude that the E-$FADH_2$·NAD^+ complex of C42S (and wild-type) Nox reacts directly with O_2. At pH 7.0 and 5 °C, the reduced enzyme·NAD^+ complex reacts with O_2 in a reversible second-order reaction:

$$\frac{\text{E-FADH}_2\cdot\text{NAD}^+}{\text{E-FADH}_2\cdot\text{NAD}^+} + O_2 \underset{56\ s^{-1}}{\overset{8.5\times10^5\ M^{-1}s^{-1}}{\rightleftharpoons}} \frac{\text{E-FADHOOH(NAD}^+)}{\text{E-FADH}_2\cdot\text{NAD}^+}$$

Before commenting on the kinetic inequivalence observed for the two $FADH_2$ per dimer, we should note that the second-order rate constant for this oxygen reaction is 3−8-fold higher than those for the respective substrate complexes of reduced PHBH (2.6×10^5 M^{-1} s^{-1} at 3.5 °C; *24*) and phenol hydroxylase (1.1×10^5 M^{-1} s^{-1} at 4 °C; *28*). Considering that Nox is, strictly speaking, a member of the GR class of disulfide reductases, the observed high rate of oxygen reactivity is remarkable; the corresponding rate constant for reduced lactate oxidase (a very efficient H_2O_2-forming flavoprotein), for comparison, is 1.3×10^6 M^{-1} s^{-1} at 4 °C (*34*). Fully reduced GR reacts only very slowly with O_2 (*35*); the O_2 reactivity of Nox must be attributable to features of the flavin environment very different from those of disulfide reductases in general. Also, although it has not been investigated in detail, the O_2 reactivity of the closely related Npx under steady-state conditions is only 4% of its peroxidatic activity at pH 7.0 (*36*).

The formation of the peroxyflavin component can be followed directly by the rapid absorbance increase at 390 nm; as with the peroxyflavin intermediates of PHBH (with 6-hydroxynicotinate; *27*) and 2-methyl-3-hydroxypyridine-5-carboxylic acid oxygenase (with substrate; *21*), this component has very little or no fluorescence. The rapid, [O_2]-dependent reaction at 660 nm is due to the loss of $FADH_2 \rightarrow NAD^+$ charge-transfer absorbance on conversion of that $FADH_2$ to FADHOOH. By comparison, it is important to note that the $NADP^+$ complex of the peroxyflavin form of microsomal FAD-containing monooxygenase exhibits no charge-transfer absorbance involving bound $NADP^+$ (*25*), either. Diode-array difference spectra show that formation of the C42S Nox peroxyflavin component corresponds to the reaction of only one $FADH_2$ per dimer, since the decrease in A_{725} is only one-half of that observed on full reoxidation. Further support for this conclusion comes from the difference spectrum obtained by subtracting the spectral component attributed to the complementary E-$FADH_2$·NAD^+ subunit; the difference spectrum gives a single maximum at 372 nm ($\epsilon = 10.7$ mM^{-1} cm^{-1}) which compares very favorably with those of the peroxyflavin spectra of PHBH ($\lambda_{max} = 382-385$ nm, $\epsilon = 8.7-9.7$ mM^{-1} cm^{-1}; *24*), 2-methyl-3-hydroxypryidine-5-carboxylic acid oxygenase ($\lambda_{max} = 385$ nm, $\epsilon = 10.2$ mM^{-1} cm^{-1}; *21*), and microsomal FAD-containing monooxygenase ($\lambda_{max} = 366$ nm, $\epsilon = 10.8$ mM^{-1} cm^{-1}; *25*). Although the combined stopped-flow fluorescence and absorbance analyses of Maeda-Yorita and Massey (*28*) allowed the kinetic distinction between anionic and protonated FADHOOH species of phenol hydroxylase, we are not able to make such a distinction for the C42S Nox component. Given the λ_{max} value of 372 nm, we would attribute the absorbance spectrum to the protonated C42S Nox FADHOOH.

The second step in the oxidative half-reaction involves formation of one H_2O_2 per dimer:

$$\frac{\text{E-FADHOOH(NAD}^+)}{\text{E-FADH}_2\cdot\text{NAD}^+} \xrightarrow{35\ s^{-1},\ H_2O_2} \frac{\text{E-FAD(NAD}^+)}{\text{E-FADH}_2\cdot\text{NAD}^+} \xrightarrow{28\ s^{-1},\ NAD^+} \frac{\text{E-FAD}}{\text{E-FADH}_2\cdot\text{NAD}^+}$$

Direct peroxide detection with HRP gives both the stoichiometry and first-order rate constant for this reaction; these values are very consistent with two of the key observations from stopped-flow analyses of enzyme reoxidation. Diode-array difference spectra show that (1) almost exactly 50% of the oxidized enzyme spectrum appears at an [O_2]-independent rate constant of 35 s^{-1} and (2) there is no change in A_{725} during this phase; i.e., there is no reaction involving the E-$FADH_2$·NAD^+ component of the dimer. There is no direct evidence from the absorbance data that NAD^+ remains bound to the primary subunit at this stage (i.e., this NAD^+ is spectrally silent). However, in comparing the kinetic data from the absorbance and fluorescence modes, we determined that a fourth kinetic phase corresponding to a rate constant of 28 s^{-1} (very similar to the rate constant of 35−38 s^{-1} measured by both absorbance and fluorescence) was necessary to fit a decrease in fluorescence over the excitation range of 340−390 nm. The structure of the Npx·NADH complex (*37*) demonstrates that the pyridine nucleotide binds on the *re* side of the isoalloxazine; the same orientation almost certainly holds for the reduced Nox·NAD^+ intermediate. NAD^+ binding thus precludes the reaction of O_2 on the *re* face, and modeling studies have led to the conclusion (*16*) that the C(4a)-peroxyflavin intermediate described in this report must involve the enantiomeric form opposite of that found in PHBH. Comparisons of free and NADH-complexed Npx (*37*) indicate that the major side chain movement on pyridine nucleotide binding involves Tyr159, which swings out on NADH binding. This Tyr (Tyr157 in Nox) is conserved within the NADH-binding fingerprint sequence for Nox as well (*6*), and almost certainly movement of the Tyr157 aromatic ring accompanies NAD^+ release from the primary subunit; this side chain movement may be responsible for the observed decrease in fluorescence at 28 s^{-1}.

The final step in reoxidation accounts for the stoichiometric oxidation of the remaining reduced flavin component; however, it must be emphasized that the rate constant for this process is independent of [O_2] ($k_{obs} = 1.4-1.9$ s^{-1} at O_2 concentrations from 0.13 to 1 mM). We conclude that the O_2 reactivity of this flavin is limited by some conformational or chemical change which is linked to the redox state of the primary subunit:

$$\frac{\text{E-FAD}}{\text{E-FADH}_2\cdot\text{NAD}^+} \xrightarrow{2\ s^{-1}} \left(\frac{\text{E-FAD}}{\text{E-FADH}_2\cdot\text{NAD}^+}\right)^*$$

$$\left(\frac{\text{E-FAD}}{\text{E-FADH}_2\cdot\text{NAD}^+}\right)^* + O_2 \xrightarrow{>>2\ s^{-1}} \frac{\text{E-FAD}}{\text{E-FAD}} + H_2O_2 + NAD^+$$

There is excellent agreement for both the stoichiometry and rate constant (1.8 s^{-1}) for H_2O_2 formation and the results from diode-array and single-wavelength analyses of enzyme reoxidation in this phase. A very similar rate constant of

1.5 s^{-1} was observed in the fluorescence analysis of this reaction; however, we conclude that there is a significant difference between the fluorescence yields of the E-FAD components common to the (E-FAD/E-$FADH_2$·NAD^+)* and E-FAD/E-FAD species. Therefore, the final phase of reoxidation accounts for about 70% of the total fluorescence increase observed over the excitation wavelength range (340−450 nm) investigated. In quantitative static fluorescence analyses of the fully oxidized (E/E) and E/EH_2 forms of wild-type Nox, we have shown that reduction of one Cys42-SOH per dimer reduces the fluorescence yield of E/EH_2 to 37% of that for the E/E dimer.[4] This demonstrates that the fluorescence of E-FAD is sensitive to the redox state of the complementary subunit, consistent with the stopped-flow fluorescence results for C42S Nox reoxidation.

To our knowledge, this description of a C(4a)-peroxyflavin intermediate in C42S Nox is the first example of such an oxygenated flavin species outside the flavoprotein monooxygenase class (e.g., PHBH; *15*). Other properties of Nox previously reported (*16*, *38*) have also been interpreted with direct reference to PHBH and other FAD-containing monooxygenases. For example, the aromatic hydroxylases do not cause dramatic spectral perturbations on binding 8-mercapto-FAD, and the resulting 8-mercapto-FAD enzymes are readily reduced by pyridine nucleotide in the presence of substrate (*39*). Nox also stabilizes the N(1)-protonated *p*-quinoid form of 8-mercapto-FAD (*16*, *38*), and this enzyme is rapidly reduced by NADH as well. Neither PHBH nor Nox stabilizes the flavin N(5)-sulfite adduct or the anionic semiquinone; PHBH can stabilize small to substantial amounts of neutral flavin semiquinone (*39*), but only in the presence of certain substrates such as 2,4-dihydroxybenzoate or tetrafluoro-*p*-hydroxybenzoate. Similarly, wild-type Nox stabilizes the blue semiquinone only when reduced in the presence of the inhibitor azide (*16*); the C42S mutant yields small amounts of neutral radical on direct reduction with NADH or dithionite. It has been pointed out by Entsch et al. (*40*) and by Gatti et al. (*41*) that the virtually 100% coupled hydroxylation of *p*-hydroxybenzoate by PHBH is the consequence of a very favorable balance between factors which dramatically reduce the lability of FADHOOH toward expulsion of H_2O_2 and at the same time enhance the reactivity of FADHOOH toward the substrate. With the mobile FAD of PHBH sequestered in the "in" conformation which is productive for hydroxylation, the C(4a)- and N(5)-loci are protected from solvent, effectively preventing formation of H_2O_2 by the peroxyflavin (*41*); a maximal H_2O_2 formation rate of 0.9 s^{-1} (3.5 °C) has been calculated for wild-type PHBH (*40*). The peroxyflavin intermediate of 1-deaza-FAD PHBH decays to yield H_2O_2 and oxidized flavin at 4.6 s^{-1}, as measured under similar conditions (*42*). Like PHBH, wild-type Nox is not designed to reduce $O_2 \rightarrow H_2O_2$; the Cys42-S^- is positioned for optimal *si* face reactivity with the peroxyflavin (*16*):

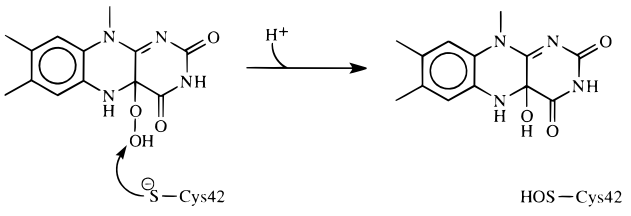

The ensuing nucleophilic attack on the distal oxygen would logically lead to direct formation of the C(4a)-hydroxyflavin. Our data with the C42S mutant indicate an intrinsic peroxyflavin decay rate ($\rightarrow H_2O_2$) of 35 s^{-1}, and it should be noted that the wild-type Nox reaction should not require activation of O_2 beyond the level of the peroxyflavin, in contrast to the additional polarization of the FADHOOH bond which is desirable for hydroxylation of aromatic substrates (*25*). Ball and Bruice (*43*) have shown that 5-ethyl-4a-peroxylumiflavin oxygenates the sulfur of thioxane (in methanol at 30 °C) with a second-order rate constant that is 10^4-fold greater than that for H_2O_2, and we have determined the second-order rate constant for H_2O_2 oxidation of the Npx Cys42-S^- (5 °C) to be 3.0×10^6 M^{-1} s^{-1} (*20*). With wild-type Nox, the rate constant for reaction of Cys42-S^- with the peroxyflavin intermediate must therefore be $\gg 35$ s^{-1}; the lability of FADHOOH is diminished to a level that is measurable only with the C42S mutant. Similar considerations for the reactivity of Cys42-S^- with the Nox peroxyflavin may account for the fully coupled (100% $O_2 \rightarrow 2H_2O$) O_2 reduction stoichiometries reported for the 1-deaza- and 2-thio-FAD reconstituted Nox enzymes, and for the absence of detectable conversion of 4-thio-FAD Nox to 4-oxo-FAD enzyme on reoxidation of the reduced enzyme (*16*).

Another direct conclusion from the spectral and kinetic analyses of the oxidative half-reaction for the dimeric C42S Nox E-$FADH_2$·NAD^+ complex is that the two subunits behave asymmetrically. Full reoxidation (and apparently NAD^+ release) at the primary subunit is followed by a rate-limiting conformational or chemical change at 2 s^{-1}; reoxidation of the complementary subunit only occurs commensurate with this latter process. The observation that a similar limiting step ($k = 1.7-1.8$ s^{-1}) is found in the reoxidations of both free and azide-bound forms of reduced C42S Nox indicates that the rate-determining step does not involve NAD^+ release. This documentation of kinetic inequivalence for the two $FADH_2$ in reduced C42S Nox complements previous observations of asymmetric behavior for wild-type Nox on reduction with either dithionite or NADH (*1*, *2*). In either case, only 1.5 equiv per FAD is required for full reduction, and one Cys42-SOH per dimer remains oxidized even in the presence of excess reductant. When the dithionite-reduced enzyme is titrated with NAD^+, about one-half of the $FADH_2$ forms a stable charge-transfer complex with NAD^+, but one $FADH_2$ per dimer is oxidized on NAD^+ binding, at the expense of the remaining Cys42-SOH (*2*). Independent evidence for active-site asymmetry in Nox also comes from analysis of the spectral and kinetic course of H_2O_2 oxidation of the 8-mercapto-FAD enzyme (*38*); flavin 8-S-oxide and 8-sulfenic acid intermediates appeared in a 50:50 mixture on initial two-electron oxidation.

While conformational changes have been described in the oxidative half-reactions of PHBH (*41*) and anthranilate hydroxylase (*22*), the kinetic inequivalence of the reduced C42S Nox flavins toward O_2 is much more relevant to that described for the C135A/C140A mutant of mercuric reductase (*44*), which lacks both Cys of the redox-active disulfide. Biphasic oxidation kinetics were observed for the asymmetric E-$FADH_2$·$NADP^+$/E-FAD·NADPH dimer with oxidation of $FADH_2$ at the primary subunit required to trigger "intramolecular" NADPH $\rightarrow$ FAD electron transfer within the complementary subunit. The second phase of reoxidation

is then observed. In this case, it is clear that asymmetry exists within the initial complexed enzyme dimers, with regard to both redox state and the identity of the bound pyridine nucleotide. With the NAD^+ complex of reduced C42S Nox, it is not evident whether there is some subtle form of preexisting asymmetry; both flavins are reduced and bound to NAD^+. A very similar spectral form predominates in steady-state turnover with NADH and O_2, and the turnover number of 2.2−2.3 s^{-1} matches the rate constant of 2 s^{-1} for the slow phase of C42S Nox reoxidation very closely; these points imply that the asymmetric behavior of Nox is relevant to the catalytic mechanism. As discussed by Miller et al. (*44*) extensively for mercuric reductase, our results with C42S Nox are also consistent with a type of alternating sites cooperativity model. With Nox, oxidation of the second subunit proceeds only after oxidation of the primary subunit; the oxygen reactivity of the second subunit is linked to the redox state of the first. Unlike the case for the mercuric reductase mutant, where the second phase of oxidation is inhibited by $NADP^+$ bound to the primary FAD, the second phase of oxidation for reduced C42S Nox·NAD^+ is limited by the conformational change of 2 s^{-1}; this process appears to provide the basis for the intersubunit communication intrinsic to the Nox version of the alternating sites cooperativity model. Mercuric reductase, like Nox and Npx, is also a member of the GR class of flavoprotein disulfide reductases (*31*); in addition to FAD and the Cys135−Cys140 redox-active disulfide, each active site (two per dimer) also includes the catalytically essential Cys558′ and Cys559′ from the complementary subunit (*44*). The crystal structure of Npx demonstrates that Phe424′ (Npx numbering; also Phe424′ in Nox) is the only residue from the complementary subunit to contribute to the active site at the primary subunit (*33*). Phe424′-O is hydrogen-bonded to the flavin N(3)-position; together with Pro426′, Pro431′, and Trp432′, this residue forms an apolar patch which shields the pyrimidine moiety of the flavin from solvent. All four of these residues from the Npx C-terminal interface domain are conserved in the four Nox sequences from enterococcal or streptococcal sources; given the role of the immediate flavin environment in controlling both $FADH_2$:O_2 reactivity and the fate of the peroxyflavin intermediate, it is interesting to speculate that a similar intersubunit contact within the Nox active site could contribute to the alternating sites cooperativity described for the oxidative half-reaction of Nox. Future mutagenesis approaches targeting these residues will be required to test this possibility.

ACKNOWLEDGMENT

We thank Dr. Derek Parsonage for developing the mutagenesis and expression protocol for C42S Nox, and we thank Dr. Parsonage and Dr. E. J. Crane for helpful discussions.

REFERENCES

1. Ahmed, S. A., and Claiborne, A. (1989) *J. Biol. Chem. 264*, 19856−19863.
2. Ahmed, S. A., and Claiborne, A. (1989) *J. Biol. Chem. 264*, 19864−19870.
3. Condon, S. (1987) *FEMS Microbiol. Rev. 46*, 269−280.
4. Higuchi, M. (1992) *Oral Microbiol. Immunol. 7*, 309−314.
5. Higuchi, M., Shimada, M., Yamamoto, Y., Hayashi, T., Koga, T., and Kamio, Y. (1993) *J. Gen. Microbiol. 139*, 2343−2351.
6. Ross, R. P., and Claiborne, A. (1992) *J. Mol. Biol. 227*, 658−671.
7. Claiborne, A., Crane, E. J., III, Parsonage, D., Yeh, J. I., Hol, W. G. J., and Vervoort, J. (1997) in *Flavins and Flavoproteins 1996* (Stevenson, K. J., Massey, V., and Williams, C. H., Jr., Eds.) pp 731−740, University of Calgary Press, Calgary, AB.
8. Yeh, J. I., Claiborne, A., and Hol, W. G. J. (1996) *Biochemistry 35*, 9951−9957.
9. Crane, E. J., III, Vervoort, J., and Claiborne, A. (1997) *Biochemistry 36*, 8611−8618.
10. Matsumoto, J., Higuchi, M., Shimada, M., Yamamoto, Y., and Kamio, Y. (1996) *Biosci., Biotechnol., Biochem. 60*, 39−43.
11. Roe, B. A., Linn, S. P., Song, L., Yuan, X., Clifton, S., McShan, M., and Ferretti, J. (1998) *Streptococcal Genome Sequencing Project*, http://dna1.chem.uoknor.edu/strep.html.
12. Parsonage, D., and Claiborne, A. (1995) *Biochemistry 34*, 435−441.
13. Crane, E. J., III, Parsonage, D., and Claiborne, A. (1996) *Biochemistry 35*, 2380−2387.
14. Claiborne, A., Miller, H., Parsonage, D., and Ross, R. P. (1993) *FASEB J. 7*, 1483−1490.
15. Massey, V. (1994) *J. Biol. Chem. 269*, 22459−22462.
16. Ahmed, S. A., and Claiborne, A. (1992) *J. Biol. Chem. 267*, 25822−25829.
17. Entsch, B., and van Berkel, W. J. H. (1995) *FASEB J. 9*, 476−483.
18. Pfleiderer, G., Jeckel, D., and Wieland, T. (1956) *Biochem. Z. 328*, 187−194.
19. Circular OR-18 (1977) P·L Biochemicals, Inc., Milwaukee, WI.
20. Crane, E. J., III, Parsonage, D., Poole, L. B., and Claiborne, A. (1995) *Biochemistry 34*, 14114−14124.
21. Chaiyen, P., Brissette, P., Ballou, D. P., and Massey, V. (1997) *Biochemistry 36*, 8060−8070.
22. Powlowski, J., Ballou, D. P., and Massey, V. (1989) *J. Biol. Chem. 264*, 16008−16016.
23. Bull, C., and Ballou, D. P. (1981) *J. Biol. Chem. 256*, 12673−12680.
24. Entsch, B., Ballou, D. P., and Massey, V. (1976) *J. Biol. Chem. 251*, 2550−2563.
25. Beaty, N. B., and Ballou, D. P. (1981) *J. Biol. Chem. 256*, 4619−4625.
26. Detmer, K., and Massey, V. (1985) *J. Biol. Chem. 260*, 5998−6005.
27. Ghisla, S., Entsch, B., Massey, V., and Husein, M. (1977) *Eur. J. Biochem. 76*, 139−148.
28. Maeda-Yorita, K., and Massey, V. (1993) *J. Biol. Chem. 268*, 4134−4144.
29. Ryerson, C. C., Ballou, D. P., and Walsh, C. (1982) *Biochemistry 21*, 2644−2655.
30. Arunachalam, U., Massey, V., and Miller, S. M. (1994) *J. Biol. Chem. 269*, 150−155.
31. Williams, C. H., Jr. (1992) in *Chemistry and Biochemistry of Flavoenzymes* (Müller, F., Ed.) Vol. III, pp 121−211, CRC Press, Boca Raton, FL.
32. delCardayré, S. B., and Davies, J. E. (1998) *J. Biol. Chem. 273*, 5752−5757.
33. Stehle, T., Ahmed, S. A., Claiborne, A., and Schulz, G. E. (1991) *J. Mol. Biol. 221*, 1325−1344.
34. Maeda-Yorita, K., Aki, K., Sagai, H., Misaki, H., and Massey, V. (1995) *Biochimie 77*, 631−642.
35. Massey, V., Müller, F., Feldberg, R., Schuman, M., Sullivan, P. A., Howell, L. G., Mayhew, S. G., Matthews, R. G., and Foust, G. P. (1969) *J. Biol. Chem. 244*, 3999−4006.
36. Poole, L. B., and Claiborne, A. (1986) *J. Biol. Chem. 261*, 14525−14533.
37. Stehle, T., Claiborne, A., and Schulz, G. E. (1993) *Eur. J. Biochem. 211*, 221−226.
38. Ahmed, S. A., and Claiborne, A. (1992) *J. Biol. Chem. 267*, 3832−3840.

39. Massey, V., Ghisla, S., and Moore, E. G. (1979) *J. Biol. Chem. 254*, 9640−9650.
40. Entsch, B., Palfey, B. A., Ballou, D. P., and Massey, V. (1991) *J. Biol. Chem. 266*, 17341−17349.
41. Gatti, D. L., Palfey, B. A., Lah, M. S., Entsch, B., Massey, V., Ballou, D. P., and Ludwig, M. L. (1994) *Science 266*, 110−114.
42. Entsch, B., Husain, M., Ballou, D. P., Massey, V., and Walsh, C. (1980) *J. Biol. Chem. 255*, 1420−1429.
43. Ball, S., and Bruice, T. C. (1979) *J. Am. Chem. Soc. 101*, 4017−4019.
44. Miller, S. M., Massey, V., Williams, C. H., Jr., Ballou, D. P., and Walsh, C. T. (1991) *Biochemistry 30*, 2600−2612.

BI9803630